Chem Soc Rev

REVIEW ARTICLE

View Article Online
View Journal | View Issue

Cite this: *Chem. Soc. Rev.*, 2023, **52**, 2528

Self-assembly of colloidal metal–organic framework (MOF) particles

Javier Fonseca,[ab] Lingxin Meng,[ab] Inhar Imaz*[ab] and Daniel Maspoch *[abc]

Self-assembly of colloidal particles into ordered superstructures enables the development of novel advanced materials for diverse applications such as photonics, electronics, sensing, energy conversion, energy storage, diagnosis, drug or gene delivery, and catalysis. Recently, polyhedral metal–organic framework (MOF) particles have been proposed as promising colloidal particles to form ordered superstructures, based on their colloidal stability, size-tunability, rich polyhedral shapes, porosity and multifunctionality. In this review, we present a comprehensive overview of strategies for the self-assembly of colloidal MOF particles into ordered superstructures of different dimensionalities, highlighting some of their properties and applications, and sharing thoughts on the self-assembly of MOF particles.

Received 23rd November 2022

DOI: 10.1039/d2cs00858k

rsc.li/chem-soc-rev

1. Introduction

Self-assembly is the process by which individual building blocks, ranging from (bio)molecules to macroscopic objects, spontaneously organise themselves into ordered superstrutures.[1] Natural self-assembly is ubiquitous and underlies the formation of many essential biological structures such as DNA, proteins, and lipid vesicles.[2–5] Beyond (bio)molecules, self-assembly of colloidal micro- or nanoscale particles into ordered superstructures has also attracted much attention due to the possibility to generate advanced materials with properties that could enable diverse applications such as photonics, electronics, sensing, energy conversion, energy storage, diagnosis, drug or gene delivery, and catalysis.[6–8] Traditionally, most colloidal ordered superstructures have been assembled from spherical or near-spherical particles of silica,[9,10] metallic

[a] *Catalan Institute of Nanoscience and Nanotechnology (ICN2), CSIC and The Barcelona Institute of Science and Technology, Campus UAB, Bellaterra, 08193, Barcelona, Spain. E-mail: inhar.imaz@icn2.cat, daniel.maspoch@icn2.cat*
[b] *Departament de Química, Facultat de Ciències, Universitat Autònoma de Barcelona, 08193 Bellaterra, Spain*
[c] *ICREA, Pg. Lluis Companys 23, 08010, Barcelona, Spain*

Javier Fonseca

Javier Fonseca obtained his bachelor's degree in Chemical Engineering from Salamanca University (Salamanca, Spain) in 2015 and his master's degree in Material Science from Rovira i Virgili University (Tarragona, Spain) in 2016. He received his PhD degree in Chemical Engineering from Northeastern University (Boston, USA) in 2020 under the supervision of Prof. Sunho Choi. He joined Prof. Chin group at University of Vienna (Vienna, Austria) as a postdoctoral researcher in 2022 and is currently a postdoctoral researcher in Prof. Maspoch's group at the Catalan Institute of Nanoscience and Nanotechnology (Barcelona, Spain). His research focuses on the design and preparation of MOF-based superstructures and MOF composites.

Lingxin Meng

Lingxin Meng received his MSc degree in Chemical Engineering from the Northeastern University (Shenyang, China) in 2021. He is currently a PhD student in Prof. Maspoch's group at the Autonomous University of Barcelona and the Catalan Institute of Nanoscience and Nanotechnology (Barcelona, Spain) thanks to a CSC scholarship. His research interests focus on controlling the size and morphology of MOF nanocrystals, their colloidal self-assembly at the mesoscale, their substantial applications (such as photonics) at the macroscale, and MOF-composites.

quantum dots (*e.g.* CdSe[11,12] and PbS[13]), metal nanoparticles (*e.g.* gold nanoparticles[14]), and polymers (*e.g.* polystyrene[15,16] and poly-(methyl methacrylate) (PMMA)).[17,18] These particles in turn generate superstructures with face-centred cubic (fcc), hexagonal close-packed (hcp), or random hexagonal close-packed (rhcp) lattices.

Progress in the controlled self-assembly of colloidal particles has recently led to the use of non-spherical, polyhedral particles based on crystalline inorganic nanoparticles (*e.g.* gold,[19] silver,[20] CdS,[21] PbSe[22] and MnO[23]),[24–27] which can adopt many polyhedral shapes such as cubic, tetrahedral, octahedral, rod-like, and rhombic dodecahedral morphologies. Compared to spherical colloidal particles, these polyhedral particles can widely expand the gamut of possible superstructures, thus providing access to new packing geometries.[28–34] For example, Mirkin *et al.* assembled ordered three-dimensional (3D) superstructures exhibiting fcc, cubic, and body-centred cubic (bcc) lattices using gold nanoparticles with rhombic dodecahedral, truncated cubic and octahedral shapes, respectively.[35] Similarly, Yang *et al.* showed the use of cubic, octahedral, and truncated octahedral silver particles to assemble 3D superstructures with cubic, space-filling Kelvin, and Minkowski-packing structures, respectively.[36]

Among the existing types of polyhedral particles, crystalline metal–organic framework (MOF) particles have very recently been postulated as new polyhedral building units to construct ordered superstructures.[37,38] As colloidal building units, MOF particles offer several advantages, which are outlined below. These characteristics make polyhedral MOF particles highly attractive for self-assembly into ordered superstructures with new properties and applications that otherwise would be inaccessible from spherical colloidal particles or other polyhedral building units.

- Polyhedral MOF particles can be an excellent source of crystalline particles that encompass most known polyhedral shapes. Consequently, their use should enable the generation of superstructures with multiple, different packings, including novel ones.
- MOFs can be obtained as colloidal particles of very homogeneous size and shape.[39–41] Furthermore, their particle size can easily be tuned from ~50 nm to ~1 μm, thus providing access to photonic crystals.
- Given that MOFs are porous, their self-assembly can yield ordered porous superstructures, thereby making them suitable for diverse applications (*e.g.* sensors).
- MOFs can exhibit various other properties (*e.g.* conductivity, chirality, magnetism, optics, *etc.*) that can lead to multifunctional ordered superstructures.
- Polyhedral MOF particles can exhibit anisotropic shapes, the self-assembly of which can enable the controlled orientation of their pores.
- Some MOF structures are flexible and will confer their flexibility to ordered superstructures.
- MOFs can be post-synthetically modified, and so can their corresponding ordered superstructures.
- MOFs can be calcinated to form inorganic and carbon-based materials, a transformation that can be used to create superstructures of these derived materials.

Several excellent reviews have been published on the self-assembly of colloidal particles, covering topics such as the principles that govern self-assembly,[42–44] the types of colloidal particles that can self-assemble,[45–47] and the characterisation, properties and applications of the resultant self-assembled superstructures.[48–50] We encourage interested readers to consult these references. Here, we examine the self-assembly of MOF particles into ordered superstructures of different dimensionalities (Table 1). We aimed to explore the recent approaches that have been exploited for creating the first ordered MOF superstructures, including solvent evaporation, depletion-assisted assembly, electric field-assisted assembly, DNA-assisted assembly, anisotropic

Inhar Imaz

Inhar Imaz received his PhD in Materials Science from the Université Bordeaux I in 2005, where he studied the formation of heterometallic metal–organic architectures from tetrahedral building blocks. He joined the CIN-2 (ICN-CSIC) centre in 2005 as a Postdoctoral fellow. At present, he is senior researcher at the Catalan Institute of Nanoscience and Nanotechnology (ICN2). His research interests are focused on controlling the supramolecular assembly of molecules, metal ions and nanoscale building blocks at the macro and nanoscale for the design of novel metal–organic frameworks and functional supramolecular architectures with interesting properties and applications in gas storage, catalysis.

Daniel Maspoch

Daniel Maspoch is an ICREA Research Professor at the Institut Català de Nanociència i Nanotecnologia (ICN2). He received his BS degree at the Universitat de Girona and his PhD degree at the Universitat Autònoma de Barcelona & Institut de Ciència de Materials de Barcelona. He worked as a postdoctoral fellow at Northwestern University. His research interests include reticular materials (MOFs, COFs and MOPs) and delivery systems.

Table 1 Superstructures assembled from colloidal MOF particles

Self-assembled superstructure	MOF particle	Reagent to screen the interactions between MOF particles	Assembly technique	Ref.
0D microsphere made of onion-like layers	C-ZIF-8 (191 ± 9 nm)	Lutensol TO-8/perfluoro-surfactant	Drying of emulsion droplets	59
0D microsphere made of onion-like layers	RD-ZIF-8 (246 ± 12, 267 ± 12, and 293 ± 13 nm)	Lutensol TO-8/perfluoro-surfactant	Drying of emulsion droplets	59
0D microsphere made of onion-like layers	TRD-ZIF-8 (181 ± 9, 198 ± 10, 229 ± 9, and 247 ± 10 nm)	Lutensol TO-8/perfluoro-surfactant	Drying of emulsion droplets	59
0D microsphere made of onion-like layers	O-UiO-66 (194 ± 12, 238 ± 13, and 247 ± 13 nm)	PVP/perfluoro-surfactant	Drying of emulsion droplets	59
0D pseudospherical photonic supraparticle	TRD-ZIF-8 (184, 206, 242, and 275 nm)	CTAB/PVA	Spray-drying of emulsion droplets	60
0D pseudospherical photonic supraparticle	TRD-ZIF-67 (193, and 205 nm)	CTAB	Spray-drying of emulsion droplets	60
0D pseudospherical photonic supraparticle	TRD-ZIF-8 (275 nm)/Au nanoparticle (51 nm)	CTAB	Spray-drying of emulsion droplets	60
0D hollow microsphere	C-Fe-soc-MOF (310 ± 10 nm)	Tween-85	Drying of emulsion droplets	61
8-c cubic cluster	O-UiO-66 (735 ± 21 nm)	PVP	Colloidal fusion synthesis	66
6-c octahedral cluster	C-ZIF-8 (205 ± 10 nm)	CTAB	Colloidal fusion synthesis	66
12-c cuboctahedral cluster	RD-ZIF-8 (526 ± 27 nm)	CTAB	Colloidal fusion synthesis	66
1D chains	RD-ZIF-8 (5.3 μm)	PVP	External electric field	71
1D chains	UiO-66-on-MIL-96 Truncated hexagonal bipyramidal MIL-96 (μm-size)	—	Anisotropic pattern	75
1D chains (on a smooth substrate)	RD-ZIF-8 (0.9 ± 0.3 μm)	CTAC	Depletion interaction in capillary	76
1D chains (on a smooth substrate)	TRD-ZIF-8 (1.2 ± 0.2 μm)	CTAC	Depletion interaction in capillary	76
1D chains (on a smooth substrate)	MIL-88A (1.6 ± 0.1 μm)	SDS	Depletion interaction in capillary	76
Anisotropic quasi-1D stripe-like superstructure (on a rough substrate)	O-UiO-66 (1.0 ± 0.1 μm)	CTAC	Depletion interaction in capillary	76
2D hexagonal lattices	RD-ZIF-8 (830 nm)	—	Solvent evaporation	38
2D snowflake-like network (on a rough substrate)	MIL-88A (1.6 ± 0.1 μm)	SDS	Depletion interaction in capillary	76
2D hexagonal lattices (on a smooth substrate)	O-UiO-66 (1.0 ± 0.1 μm)	CTAC	Depletion interaction in capillary	76
2D square lattices (on a smooth substrate)	Truncated hexagonal bipyramidal MIL-96 degree of truncation = 0.24 (1.0 ± 0.1 μm)	CTAC	Depletion interaction in capillary	76
2D centered rectangular lattices (on a smooth substrate)	Truncated hexagonal bipyramidal MIL-96 degree of truncation = 0.52 (0.8 ± 0.1 μm)	CTAC	Depletion interaction in capillary	76
2D hexagonal lattices	TC-In-soc-MOF (1.60 ± 0.04 μm)	PVP	Solvent evaporation	79
2D simple cubic lattices	C-Ga-soc-MOF (360 ± 20 nm)	PVP	Solvent evaporation	79
2D hexagonal lattices	TRD-ZIF-8 (174 ± 15 nm)	CTAB/PMMA	Air–liquid interface	80
2D hexagonal lattices	O-UiO-66 (409 ± 29 nm)	PVP/SDS	Air–liquid interface	81
2D films	HKUST-1	—	LB	82
2D films	$Al_{12}O(OH)_{18}(H_2O)_3(Al_2(OH)_4)(BTC)_6$	—	LB	82
2D films	$Cu_2(BDC)_2(bipy)$	—	LB	82
2D hexagonal lattices	O-UiO-66 (80 nm)	PBnMA	Air–liquid interface	84
2D hexagonal lattices	O-UiO-66 (80 nm)	PMA	Air–liquid interface	84
2D hexagonal lattices	O-UiO-66 (120 nm)	PMA	Air–liquid interface	84
2D hexagonal lattices	RD-ZIF-8 (590, and 745 nm)	PVP	LB	89
2D simple cubic lattices	TC-ZIF-8 (600 nm)	PVP	LB	89
2D hexagonal lattices	TRD-ZIF-8 (500 nm)	PVP	LB	89
2D hexagonal lattices	PCN-222 nanorods (38 ± 8 nm × 159 ± 25 nm)	—	Anisotropic pattern (oligonucleotides) [self-complementary DNA sticky ends]	90
2D tetragonal lattices	PCN-222 nanorods (38 ± 8 nm × 159 ± 25 nm)	—	Anisotropic pattern (oligonucleotides) [complementary DNA sticky ends]	90
2D quasi-ordered superstructures	TRD-ZIF-8 (182 ± 11 nm)	CTAB	Ice-templating strategy	92
2D quasi-ordered superstructures	C-ZIF-8 (150 ± 12 nm)	—	Ice-templating strategy	92
2D quasi-ordered superstructures	O-UiO-66 (from 300 to 800 nm)	—	Ice-templating strategy	92
2D quasi-ordered superstructures	MIL-88B(Fe)-NH_2 hexagonal nanorods (300 nm)	—	Ice-templating strategy	92
3D rhombohedral packing	TRD-ZIF-8 (TRD-ZIF-8) degree of truncation >0.66 (210 ± 10 nm)	CTAB	Solvent evaporation	37
3D fcc packing	TRD-ZIF-8 (TRD-ZIF-8) degree of truncation <0.66 (263 ± 13 nm)	CTAB	Solvent evaporation	37
3D hexagonal packing	O-UiO-66 (340 ± 30 nm)	CTAB	Solvent evaporation	37
3D superstructures	NU-1000 (length-to-diameter ratio = 3.4 ± 0.2)	TMPTA	External electric field	70

Table 1 (*continued*)

Self-assembled superstructure	MOF particle	Reagent to screen the interactions between MOF particles	Assembly technique	Ref.
3D superstructures	MIL-68(In) (length-to-diameter ratio = 6.8 ± 0.9) (length-to-diameter ratio = 1.2 ± 0.2)	TMPTA	External electric field	70
3D superstructures	MIL-53-NH_2(Al) (length-to-diameter ratio = 10 ± 5)	TMPTA	External electric field	70
Quasi-3D superstructures (on a rough substrate)	RD-ZIF-8 (0.9 ± 0.3 μm)	CTAC	Depletion interaction in capillary	76
3D hexagonal packing	O-UiO-66 (409 ± 29 nm)	PVP	Solvent evaporation	81
3D fcc packing	O-UiO-66 (86 ± 10 nm)	—	Anisotropic pattern (oligonucleotides) [self-complementary DNA sticky ends]	90
3D bcc packing	O-UiO-66 (86 ± 10 nm)	—	Anisotropic pattern (oligonucleotides) [complementary DNA sticky ends]	90
3D CsCl-type lattices	Spherical UiO-66 (37 ± 8 nm)/spherical Au nanoparticle (40 nm)	—	Anisotropic pattern (oligonucleotides) [complementary DNA sticky ends]	90
3D CsCl-type lattices	Spherical UiO-66 (37 ± 8 nm)/spherical Au nanoparticle (20 nm)	—	Anisotropic pattern (oligonucleotides) [complementary DNA sticky ends]	90

Notation: cubic (C); rhombic dodecahedral (RD); truncated rhombic dodecahedral (TRD); octahedral (O); cetyltrimethylammonium bromide (CTAB); cetyltrimethylammonium chloride (CTAC), polyvinyl alcohol (PVA); polyvinylpyrrolidone (PVP); poly-(methyl methacrylate) (PMMA); poly-(benzyl methacrylate) (PBnMA); poly-(methyl methacrylate) (PMA); sodium dodecyl sulphate (SDS); Langmuir–Blodgett (LB); truncated cubic (TC); face centred-cubic (fcc); body centred-cubic (bcc); trimethylolpropane triacrylate (TMPTA).

pattern-assisted assembly, ice-templated self-assembly, and air–liquid interface assembly. To help the reader navigate this review, we have organised each assembled superstructure here by dimensionality. We conclude by providing our thoughts on MOF particle self-assembly, potential applications of prepared superstructures, and current challenges in the field.

2. From uniform colloidal MOF particles to ordered superstructures

Before discussing the approaches to create ordered MOF superstructures, we first present an overview of the fundamentals of the self-assembly of colloidal MOF particles. We begin by discussing the preparation of uniform colloidal MOF particles, then explain the forces that govern these colloidal dispersions, and close by exploring the interparticle forces that influence the self-assembly (Fig. 1).

The preparation of colloidal MOF particles of uniform size and morphology forms the basis of experiments on MOF-based self-assembly. Accordingly, researchers are constantly seeking to expand the library of uniform colloidal MOF particles accessible for experimental work.[51,52] The importance of synthetic parameters (*e.g.* precursors, modulators, reaction time, and reaction temperature) on the preparation of colloidal MOF particles has been revealed over the past two decades.[39,41] For example, nucleation and growth rates have been found to define the size of the resultant MOF particles. Thus, the formation of colloidal MOF particles of uniform size is usually successful when nucleation is favoured over growth. Generally, an excess of ligand promotes nucleation, leading to small, uniform MOF particles. Another influential factor in the preparation of colloidal MOF particles with uniform size is the modulators used, as they can modify the nucleation and the growth rates.[53] On the other hand, the shape of the MOF particles is defined by the most thermodynamically stable facet orientation. In this regard, the use of surfactants is a common approach to control the morphology of MOF particles, as they selectively adhere to certain specific crystalline facets, thereby inhibiting growth at those facets. The shape of MOF particles can also be controlled post-synthetically by top-down strategies such as wet-chemical etching.[54]

Once uniform colloidal MOF particles have been prepared, their colloidal stability must be ensured to enable their self-assembly into superstructures. A colloidal dispersion of uniform MOF particles is stable when the interparticle interaction is repulsive. Thus, MOF-based colloidal solutions become destabilised when interparticle interactions change from repulsive to attractive, which results in an unbalanced and uncontrolled MOF flocculation. Typically, the van der Waals attractive interaction among MOF particles favours their flocculation. There are two different mechanisms to screen van der Waals interactions and stabilise colloidal MOFs: steric stabilisation, by tethering molecular chains to the MOF;[55,56] and electrostatic stabilisation, by adjusting the surface charge of the MOF.[57] In the first mechanism, the osmotic and elastic repulsion among the ligand coronas that tether the MOF particles cause the steric stabilisation of the particles. In the second mechanism, surface-charged MOF particles are neutralised by oppositely charged counterions, which promotes the formation of an electrical double-layer. The overlapping of the electrical clouds of MOF particles generates an osmotic repulsion among them, thus screening their van der Waals interaction.

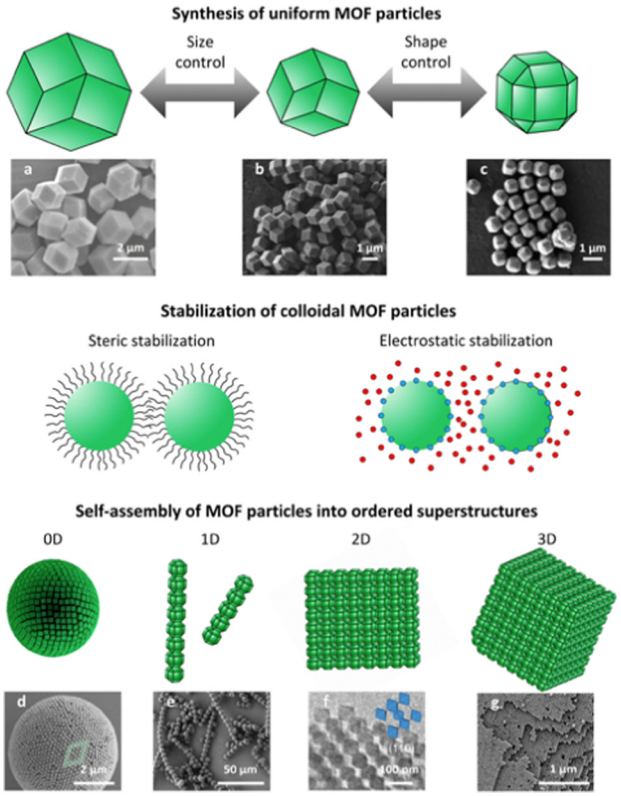

Fig. 1 Schematic of the self-assembly of MOF particles, including the synthesis of uniform MOF particles, the stabilisation of colloidal MOF particles and finally, the self-assembly of MOF particles into ordered superstructures. SEM images of colloidal RD-ZIF-8 particles sized (a) 2 μm or (b) 1 μm, and (c) colloidal TRD-ZIF-8 particles sized 500 nm. SEM images of (d) a 0D superstructure of TRD-ZIF-8 particles, (e) 1D superstructures of MOF-based patchy particles, and (g) a 3D superstructure of TRD-ZIF-8 particles. (f) TEM image of a 2D superstructure of O-UiO-66 particles. Adapted with permission from ref. 51, copyright 2018 American Chemical Society; ref. 52, copyright 2011 American Chemical Society; ref. 59, copyright 2022 John Wiley and Sons; ref. 75, copyright 2021 John Wiley and Sons; ref. 90, copyright 2020 Springer Nature; and ref. 37, copyright 2017 Springer Nature.

Having highlighted the forces that govern the preparation of MOF-based colloidal dispersions, we would like to underscore that these and other interparticle forces must be considered in the self-assembly of MOF colloidal particles. Notably, the physicochemical properties of MOF particles (*e.g.* size, shape, surface charge, high porosity, low density, *etc.*) and the physicochemical properties of the molecular chains that tether the MOFs (*e.g.* length, charge, hydrophobicity, density, molecular weight, *etc.*) strongly influence the interactions among MOF particles during self-assembly. For example, charged MOF particles exhibit electrostatic interactions. Other forces may also be present, depending on the self-assembly methodology employed (*e.g.* solvent evaporation, depletion-assisted assembly, electric field-assisted assembly, DNA-assisted assembly, anisotropic pattern-assisted assembly, ice-templated self-assembly, and air–liquid interface assembly). For example, when evaporation is used, gravity may be a plausible driving force for large MOF particles. Given the abundance of interactions and the unknown contribution of each term, accurately reporting on the interactions among MOF particles in self-assembly is extraordinary difficult. In fact, the interactions among MOF particles in the self-assembly have not yet been explored in any study. However, since self-assembly occurs under near-equilibrium conditions,[58] in which the interparticle attractions remain comparable to the thermal energy (k_BT; where k_B is the Boltzmann constant, and T is the temperature) of the system, we consider that understanding and modelling the interparticle interaction will contribute to the success of the self-assembly.

3. Self-assembly of metal–organic framework particles into zero-dimensional ordered superstructures

Self-assembly of colloidal particles into zero-dimensional (0D) ordered superstructures usually occurs in confined nano- or microscale spaces, typically in nano- or microdroplets. These spaces restrict the freedom of movement of the particles, which could favour their self-organisation and ultimately self-assembly. Two techniques are used to induce self-assembly of 0D MOF superstructures within droplets: solvent evaporation at the surface of emulsion droplets; and spray-drying.[59,60]

In 2013, Eddaoudi *et al.* pioneered the formation of 0D superstructures *via* drying of emulsion droplets. These superstructures were hollow microspheres comprising a monolayer shell of cubic Fe-soc-MOF (C-Fe-soc-MOF) particles (Fig. 2(a)–(d)).[61] Interestingly, the authors named these superstructures colloidosomes, and such structures are also known as supraballs or supraparticles.[62,63] They prepared monodisperse C-Fe-soc-MOF particles in the presence of *tert*-butylamine, which acted as structure-directing agent, and of polyoxyethylene (20) sorbitan trioleate (also known as tween-85), which acted as emulsifier. This ultimately led to spontaneous formation of hollow superstructures in two steps: firstly, emulsified droplets were formed, and subsequently, the monodispersed C-Fe-soc-MOF cubes were synthesised and spontaneously assembled at the interface of the droplets. Self-assembly occurred as those droplets evaporated. The dimensions of the emulsion droplet and consequently, of the final superstructure, were found to depend on the amount of emulsifier. Thus, the diameter of the hollow colloidosomes was inversely proportional to the amount of tween-85. The smaller hollow colloidosomes were more rigid, a phenomenon that the authors attributed to the stabilisation that was achieved when more emulsifier had been used.[61]

More recently, cubic ZIF-8 (C-ZIF-8), rhombic dodecahedral ZIF-8 (RD-ZIF-8), truncated rhombic dodecahedral ZIF-8 (TRD-ZIF-8), and octahedral UiO-66 (O-UiO-66) particles have also been self-assembled *via* drying of emulsion droplets.[59] These MOF particles self-assembled into spherical, onion-like ordered superstructures that exhibit structural colour. Unlike the study discussed above, in which hollow colloidosomes were reported to have formed during the synthesis of MOF particles, the formation of these colloidal 0D superstructures occurred from the controlled assembly of pre-synthesised MOF particles.

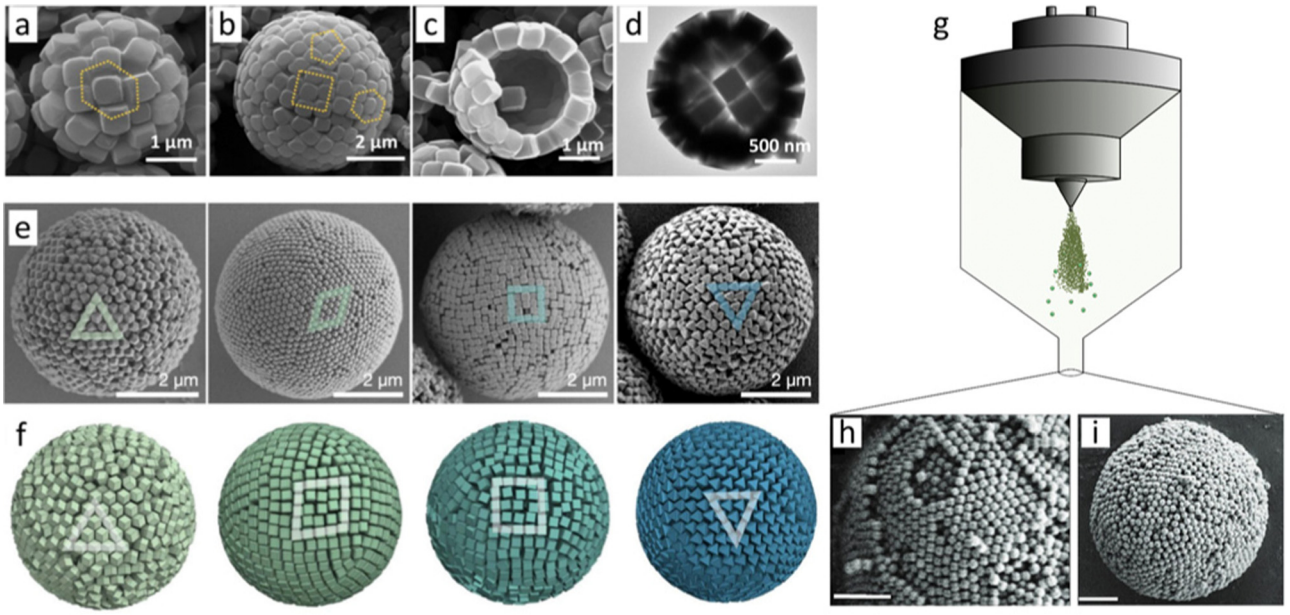

Fig. 2 (a)–(c) SEM and (d) TEM images of hollow colloidosomes assembled from C-Fe-soc-MOF particles (edge length of ~310 ± 10 nm). The estimated hollow diameter was from 3 to 5 μm. Adapted with permission from ref. 61. Copyright 2013 American Chemical Society. (e) FESEM images of spherical, onion-like ordered superstructures made of RD-ZIF-8, TRD-ZIF-8, C-ZIF-8, or O-UiO-66 particles. (f) Monte Carlo simulations of hard polyhedra in spherical confinement. These simulations matched the experimental packings. Adapted with permission from ref. 59. Copyright 2022 John Wiley and Sons. (g) Schematic of the preparation of photonic supraparticles by self-assembly of MOF particles *via* spray-drying. (h) SEM image of a ZIF-8 photonic supraparticle. Scale bar: 1 μm. (i) SEM image of a ZIF-8/PVA photonic supraparticle. Scale bar: 2 μm. Adapted with permission from ref. 60. Copyright 2021 John Wiley and Sons.

Initially, stable colloidal solutions of ZIF-8 and UiO-66 particles were prepared using Lutensol TO-8 and polyvinylpyrrolidone (PVP), respectively. These colloidal dispersions were then emulsified in perfluorinated oil using ultrasound or microfluidics, and the resulting droplets were stabilised with a perfluoro-surfactant. Onion-like layered superstructures were finally obtained by drying the emulsion droplets. The different MOF particles packed differently on the surface of these superstructures (Fig. 2(e) and (f)). Thus, C-ZIF-8 particles formed a square unit-cell; RD-ZIF-8 and O-UiO-66 particles, a triangular unit-cell; and TRD-ZIF-8 particles, a rhombic unit-cell. The planar faces of the MOF particles were suggested to align along the droplet interface, thus forming the outer layer of the superstructure. Similarly, the MOF particles underneath formed another ordered layer following the curvature of the outer layer and so on. Therefore, the superstructures were proposed to exhibit an onion-like order under the surface, the thickness of which depended on the tendency of the different MOF particles to self-assemble when confined in the spherical droplet.[59]

The spray-drying technique, which is based on atomised droplet drying,[64] has been reported to induce self-assembly of MOF particles. Instead of forming perfect spherical superstructures,[59,61] spray-drying has led to self-assembly of colloidal MOF particles into pseudospherical photonic superstructures (Fig. 2(g)–(i)).[60] Specifically, ZIF-8, ZIF-67 and ZIF-8/Au nanoparticles composite photonic superstructures were prepared by spray-drying emulsion droplets. The pseudo-sphericity was caused by the preference of faceted polyhedral MOF particles to self-assemble into faceted superstructures with the densest possible packing. The larger droplets, as well as the smaller MOF particles, favoured the formation of curved photonic superstructures. Interestingly, spray-drying dries the generated droplets almost instantly,[64,65] which tends to induce buckling or crumpling effects.[60]

Beyond spherical 0D superstructures, another type of 0D superstructures are colloidal clusters (also known as colloidal molecules), in which a small number of colloidal particles are arranged in organised geometric systems resembling a "cluster" or a "molecule". Recently, the polyhedral shape of colloidal MOF particles has also been used to direct the assembly of colloidal clusters. For this assembly, MOF particles act as core particles to direct the assembly of spherical polystyrene particles (Fig. 3).[66] This approach is based on attaching a single spherical polystyrene particle to each face of a polyhedral particle *via* colloidal-fusion synthesis.[67] Accordingly, the faces of the MOF particle define the final coordination number and geometry of the assembled colloidal cluster. Using this approach, octahedral, cubic and cuboctahedral clusters were assembled using C-ZIF-8, O-UiO-66 and RD-ZIF-8 core particles, onto which 6, 8 and 12 polystyrene spherical particles were attached, respectively.

4. Self-assembly of metal–organic framework particles into one-dimensional ordered superstructures

The assembly of one-dimensional (1D) MOF particle superstructures (also known as chains) requires that MOF particles

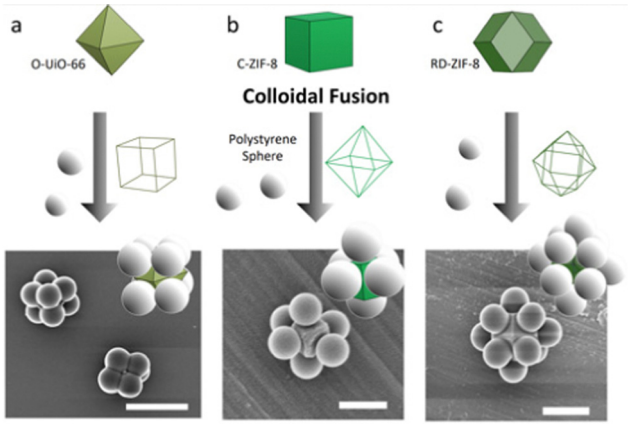

Fig. 3 Schematic of the colloidal-fusion strategy, and corresponding SEM images of (a) an 8-c cubic cluster, (b) a 6-c octahedral cluster, and (c) a 12-c cuboctahedral cluster. Scale bars: (a) 2 μm; (b) 300 nm; and (c) 1 μm. Adapted with permission from ref. 66. Copyright 2021 American Chemical Society.

be correctly aligned. One way to promote alignment is through the use of electric and magnetic fields.[68–70] Specifically, electric fields have been shown to induce self-assembly of RD-ZIF-8 particles into 1D superstructures: for instance, in polarising the electrostatic double layer on the surface of ZIF-8 particles.[71] Dipole–dipole interaction between electrostatic double layers of ZIF-8 particles led to surface-to-surface contact of the particles,[71–74] which resulted in the formation of 1D chains along the electric-field direction (Fig. 4(a) and (b)). When ZIF-8 particles self-assembled in a low frequency (1 kHz) electric field, in which the dominant attraction mechanism is electrostatic double-layer polarisation, the particle chains remained stable even after the electric field had been turned off. However, when assembled in a high frequency (1 MHz) electric field, where dielectric polarisation of the crystal particle itself dominates, the corresponding 1D superstructures were not stable.[72,73] Moreover, the chains also fell apart when the facets of ZIF-8 particles exhibited curvature.[71]

Another way of controlling the assembly of 1D superstructures is based on the use of Janus MOF particles, whose two opposing surface sides differ in composition. If there is an attractive interaction between the two sites, then this can be exploited for controlled assembly of the particles into 1D superstructures. Such is the case of the formation of 1D particle chains using MOF-based patchy particles (also called UiO-66-on-MIL-96 particles).[75] These particles were synthesised by selectively growing UiO-66 on the (0002) facets of truncated hexagonal bipyramidal MIL-96 particles. This heteroepitaxial growth was favoured by the close match of the (0002) planes of MIL-96 and the (111) planes of UiO-66. Then, 3-(trimethoxysilyl)propyl methacrylate oligomers (o-TPM) were deposited as a thin liquid layer on the UiO-66 patches, whereas o-TPM deposition on the MIL-96 surface was completely suppressed. Consequently, o-TPM acted as a glue between UiO-66 patches of two particles, thus maximising their contact and leading to the formation of 1D particle chains (Fig. 4(c)–(g)).[75] This strategy, referred to as anisotropic pattern-assembly, is limited by the difficulty of preparing Janus MOF particles with surfaces that contain the necessary information to guide the assembly in a controlled manner. Importantly, anisotropic pattern-assembly encodes assembly information locally, through short–ranged interactions, unlike other approaches, in which constraints are used to direct the assembly of MOF particles.

Wang *et al.* have recently developed ordered superstructures with different dimensionalities, by destabilising the colloidal solution through the depletion interaction within a capillary.[76] The depletion interaction fosters the short–range attractive force among colloids.[77,78] Specifically, this attractive force arises among colloidal particles when they are diluted in solution together with small, non-interacting co-solutes called depletants (*e.g.*, small nanoparticles, micelles, polymers, salts, *etc.*).[76] An effective osmotic pressure appears when two particles approach each other at a separation distance shorter than the size of the depletants. This osmotic pressure causes the particles to assemble. Furthermore, self-assembly increases the free volume for the depletants to move, thus increasing the entropy of the system. In the study by Wang and colleagues, cetyltrimethylammonium chloride (CTAC) and sodium dodecyl sulphate (SDS) facilitated the self-assembly of different MOF particles (RD and TRD-ZIF-8 particles, hexagonal rods of MIL-88A, O-UiO-66 particles, and truncated hexagonal bipyramidal MIL-96 particles) in an aqueous environment inside a capillary. Researchers have suggested that these surfactants induce a depletion interaction among the MOF particles. Furthermore, they found that different parameters (the size and shape of the MOF particles, the interactions among MOF particles and the substrate, and the degree of truncation of MOF particles) can alter the dimension and organisation of the resulting MOF superstructures. Specifically, while RD-ZIF-8 (0.9 μm) particles were found to self-assemble into quasi-3D fcc superstructures (Fig. 6(e)), RD-ZIF-8 (2.6 μm) and TRD-ZIF-8 (1.2 μm) particles rearranged into 1D chains (Fig. 4(h) and (i)). These results evidenced the influence of the size and shape of the MOF particles on the dimension of the final superstructure. The interaction among the MOF particles and the substrate (whether smooth or rough) was also reported to affect the dimension of the final superstructure. Smooth substrates led to self-assembly of MIL-88A hexagonal rods into 1D chains (Fig. 4(j)), whereas rough substrates led to rearrangement of MOF particles into two-dimensional (2D) snowflake-like superstructures. Similarly, a smooth substrate led to rearrangement of O-UiO-66 particles into 2D hexagonal lattices, but a rough substrate favoured self-assembly of a quasi-1D stripe-like superstructure.[76]

5. Self-assembly of metal–organic framework particles into two-dimensional ordered superstructures

Initial efforts to self-assemble 2D MOF particle superstructures were focused on controlling the evaporation of a colloidal

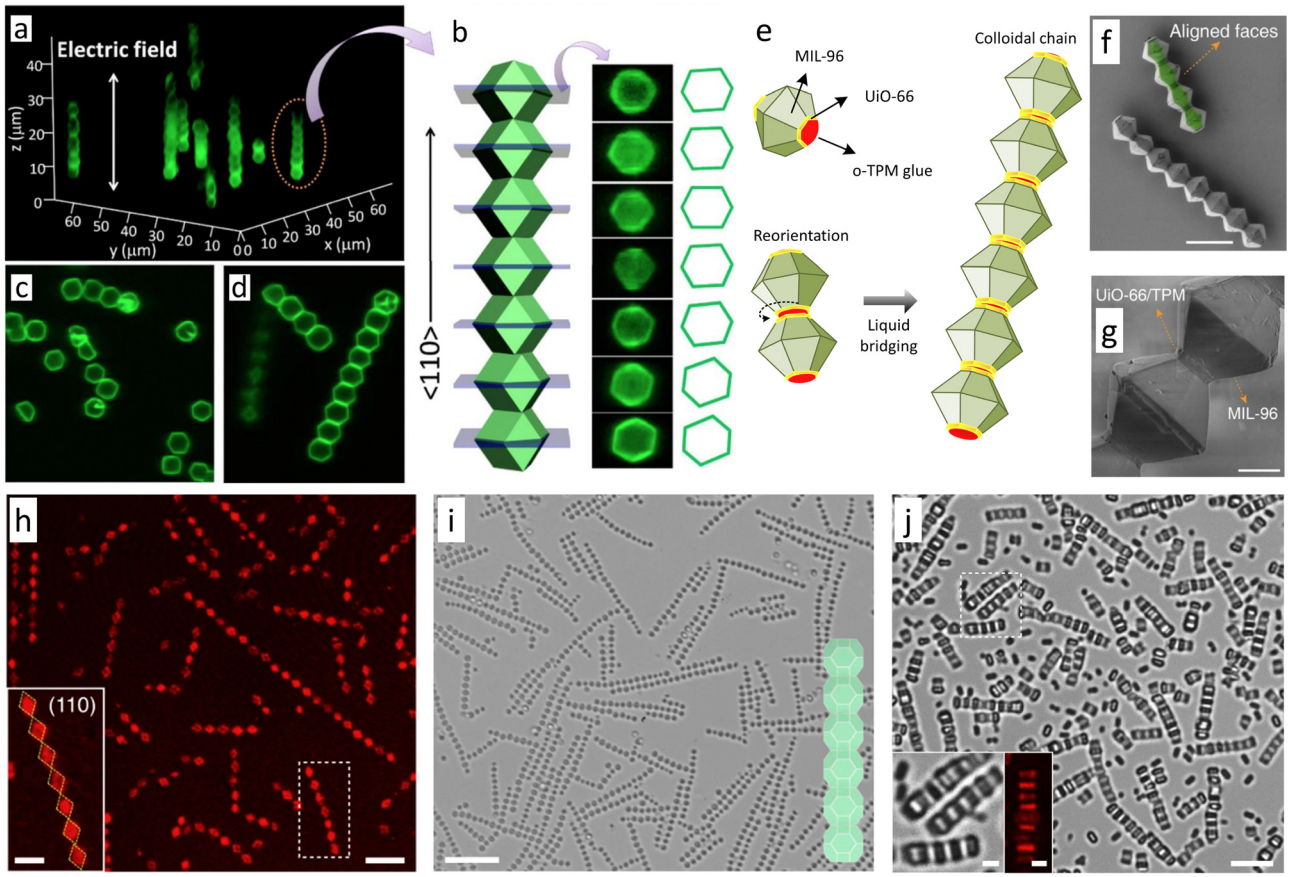

Fig. 4 Confocal microscopy of (a), (c) and (d) 1D chains of RD-ZIF-8 particles in the direction of the electric field (1 MHz). (b) Cross-sections perpendicular to the electric field. Adapted with permission from ref. 71. Copyright 2013 American Chemical Society. (e) Schematic of the self-assembly of MOF-based patchy particles. (f and g) SEM images of chains made of self-assembled, MOF-based patchy particles. Scale bars: (f) 10 μm; (g) 2 μm. Adapted with permission from ref. 75. Copyright 2021 John Wiley and Sons. (h) Confocal microscopy of 1D chains of TRD-ZIF-8 particles. Inset is the zoomed-in image of a chain. (i) SEM image of chains made of self-assembled TRD-ZIF-8 particles. (j) Optical image of chains of MIL-88A particles formed on a smooth substrate. Inset is the zoomed-in image of the chains. Scale bars: (h) 5 μm; (h, inset) 2 μm; (i) 10 μm; (j) 5 μm; (j, insets) 1 μm. Adapted with permission from ref. 76. Copyright 2022 Springer Nature.

solution containing the MOF particles. Using this approach, the Granick group and the Eddaoudi group simultaneously reported the feasibility of ordering MOF particles into 2D superstructures (usually called layers or films). Granick *et al.* showed that 2D hexagonal lattices could be assembled by slow evaporation of a colloidal solution of RD-ZIF-8 particles in *N*,*N*-dimethylformamide (DMF).[38] In ethylene glycol and using sodium nitrate to screen electrostatic repulsions between particles, colloidal RD-ZIF-8 particles were found to assemble into linear, triangular, and U-shaped trimers, linear, rhombic, and square tetramers, and fcc-lattice portions.[38] Similarly, Eddaoudi *et al.* demonstrated that the evaporation of colloidal solutions of cubic particles of M^{III}-based MOFs with square-octahedral (soc) topology (In-soc-MOF and Ga-soc-MOF) containing surfactants (*e.g.* PVP) led to the formation of 2D hcp and square close-packed layers.[79] Importantly, the evaporation assembly is mainly based on entropic crystallisation. Since the evaporation of the solvent is entropically unfavourable, the MOF particles pursue an ordered phase to maximise entropy and therefore, to minimise free energy. Further evaporation of the solvent ultimately fixes the MOF particles into ordered superstructures.

Other approaches have recently been developed to improve the 2D-ordering of MOF particles. Among the most important of these methods is air–liquid interface assembly (Fig. 5(a)), which entails first spreading a colloidal solution of MOF particles over an air–liquid interface, and then modifying the interface to drive the assembly and packing of the particles. Methods to alter the interface to favour the contact, assembly and/or packing of MOF particles include evaporation, increasing the surface tension of the liquid,[80,81] and compressing the MOF particles floating on the liquid subphase.[82] The process of spreading particles over an air–liquid interface, and then compressing them into a highly condensed state, is known as the Langmuir–Blodgett (LB) process (Fig. 5(d)).[83] Examples of such work include the formation of 2D ordered superstructures *via* self-assembly of monodisperse TRD-ZIF-8 particles on an air–liquid interface, reported by Cohen *et al.*[80] Core–shell ZIF-8 particles (PMMA@ZIF-8) were made by growing a layer of PMMA on the ZIF-8 particle. A colloidal toluene solution of these PMMA@ZIF-8 particles was then spread on water. Afterwards, evaporation of toluene induced the 2D assembly of

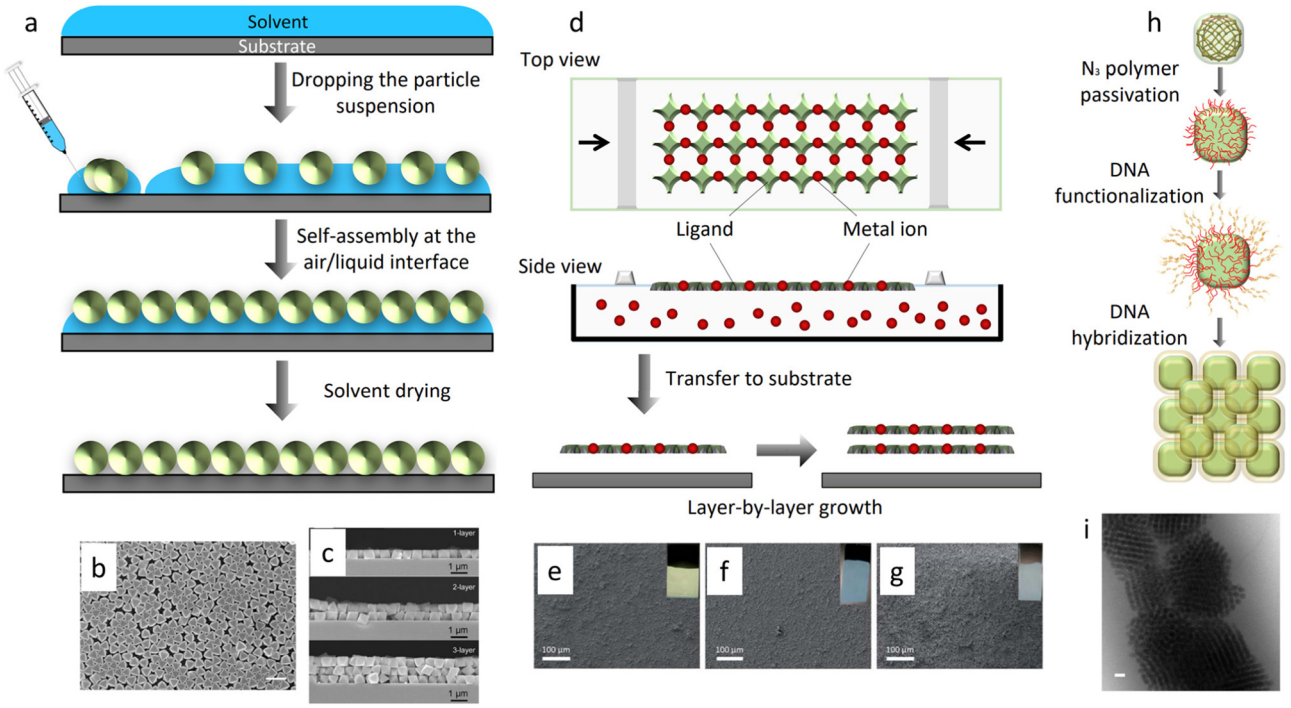

Fig. 5 (a) Schematic of air–liquid interface assembly. (b) SEM image of a 2D monolayer of O-UiO-66 crystals transferred to a silicon platform. (c) Cross sectional SEM image of one, two, and three monolayers of O-UiO-66 crystals. Scale bar: (b) 1 μm. Adapted with permission from ref. 81. Copyright 2013 John Wiley and Sons. (d) Schematic of Langmuir–Blodgett assembly. SEM images and optical microscopic images (inset) of (e)–(g) $Al_{12}O(OH)_{18}(H_2O)_3(Al_2(OH)_4)(BTC)_6$ crystals assembled by the LB process on (e) gold substrate, (f) silicon wafer and (g) glass slide. Adapted with permission from ref. 82. Copyright Royal Society of Chemistry 2012. (h) Schematic of the assembly of colloidal MOF particles *via* complementary oligonucleotides. (i) Bright field (BF) cryo-STEM image of bcc lattices formed by the assembly of O-UiO-66 crystals with self-complementary DNA sticky ends. Scale bar: (i) 100 nm. Adapted with permission from ref. 90. Copyright 2020 Springer Nature.

PMMA@ZIF-8 particles at the air–liquid interface. The resulting 2D particle films were free-standing, due to fusion of PMMA@-ZIF-8 shells. Monodispersed O-UiO-66 particles have also been self-assembled into 2D ordered superstructures on an air–liquid interface (Fig. 5(b) and (c)).[81] First, PVP-modified UiO-66 particles were spread over water. Subsequently, the surface tension of water was modified by adding an aqueous solution of SDS, leading the UiO-66 particles to consolidate into a 2D hexagonal monolayer. The presence of disorder within this monolayer was ascribed to the rapid packing of UiO-66 particles after the addition of SDS.[81] Very recently, Cohen *et al.* investigated the effects of the molecular chains attached to O-UiO-66 particles on the formation of free-standing self-assembled UiO-66 monolayers.[84] Firstly, they grafted O-UiO-66 particles of three different sizes (80 nm, 120 nm, and 250 nm) with different polymers (poly-[methyl acrylate] [PMA], PMMA, and poly-[benzyl methacrylate] [PBnMA]) at different molecular weights. Subsequently, the grafted particles self-assembled at the air–water interface. When O-UiO-66 particles were grafted with polymers of high molecular weight and density brush, certain mechanical properties (toughness and flexibility) of the monolayers improved. Since greater particle size generates larger spaces among the particles, it also negatively correlates with the mechanical properties of the monolayers. The degree of order within the monolayers was found to depend on the length and hydrophilicity of the graft as well as on the size of the O-UiO-66. Thus, order was lost when the grafts became longer or strongly hydrophilic. Regarding particle size, the larger particles favoured the formation of ordered, 2D hexagonal lattices.[84] Kitagawa, Furukawa, and co-workers assembled monodispersed MOF [HKUST-1, $Al_{12}O(OH)_{18}(H_2O)_3(Al_2(OH)_4)(BTC)_6$, and $Cu_2(BDC)_2(bipy)$] particles into 2D ordered superstructures by the LB process (Fig. 5(e)–(g)).[82] A colloidal suspension of such MOF particles in dry methanol was spread over water giving rise to a temporary bilayer of alcohol and water. MOF particles were then assembled, by compression along the air–liquid interface, into 2D ordered superstructures floating on the water subphase.[82] The assembly of MOF particles was suggested to be induced by interparticle attractive forces and capillary forces on the water sub-phase.[85–88] The LB process has also been applied to assemble PVP-modified RD, slightly truncated cubic (TC), and TRD-ZIF-8 particles into 2D monolayers. Within the monolayers, the RD particles were oriented along the [110] axis, and the TC ZIF-8 particles, along the [100] axis. Contrariwise, the TRD-ZIF-8 particles did not exhibit any unique orientation within the monolayers.[89]

Another approach to assemble colloidal MOF particles into 2D and 3D superstructures (Fig. 5(h) and (i)) is by harnessing the interactions between complementary oligonucleotides.[90,91] DNA-modified colloidal MOF particles self-assemble in a very controlled manner, as hydrogen bonding between DNA base pairs is a

highly specific interaction.[92,93] Using this chemistry, 2D close-packed hexagonal lattices have been assembled from PCN-222 nanorods functionalised with self-complementary DNA sticky ends (5′-GCGC). The use of two sets PCN-222 nanorods functionalised with complementary DNA sticky ends (5′-AAGGAA and 5′-TTCCTT) drove the formation of 2D tetragonal lattices. Similarly, DNA-functionalised O-UiO-66 particles containing self-complementary DNA linkers self-assembled into 3D fcc superstructures. By extension, two sets of O-UiO-66 particles functionalised with complementary DNA sticky ends self-assembled into 3D bcc superstructures.[90]

In another, very recent example, TRD-ZIF-8, C-ZIF-8, O-UiO-66 and hexagonal nanorods of MIL-88B(Fe)-NH_2 were self-assembled into 2D quasi-ordered superstructures using an ice-templating strategy.[94] Aqueous suspensions of MOF particles were initially frozen in liquid N_2 and, during this freezing stage, the formed polycrystalline ice pushed the MOF particles into the channels between adjacent ice crystals. Then, self-assembly of MOF particles was induced by freeze-drying. Van der Waals forces held the MOF particles together after sublimation of the ice templates. Using this strategy, mono- and bilayer 2D quasi-ordered superstructures could be created depending on the initial concentration of the MOF colloids.[94] Remarkably, these layers could be calcinated without losing their initial 2D shape, to form mono- and bilayers of 2D hollow carbon particles that exhibited a high oxygen-reduction catalytic activity in alkaline media. Given the assemblies obtained at the air–liquid interfaces,[81] emulsion droplets,[59] capillaries,[76] and ice-templates,[94] one can conclude that these approaches performed by confining MOF particles to pre-engineered interfaces provide a high level of control over self-assembly. Importantly, these methodologies allow for free movement of MOF particles within the interface, which in turn serves to correct any defects, thereby leading to the formation of energetically favourable ordered superstructures. The dimensionality of the interface usually conditions the dimensionality of the superstructures. Thus, while MOF particles generally assemble into 2D superstructures when air–liquid interfaces are used, 0D superstructures are formed when emulsion droplets are used. Interface-assisted MOF self-assembly often needs to be combined with other self-assembly approaches, such as those based on evaporation or depletion. In these cases, both the driving force and the interface define self-assembly.

As mentioned in the previous section, 2D superstructures can also be prepared by destabilising the colloidal solution through the depletion interaction inside a capillary.[76] In this study, the final superstructures were found to be influenced by the degree of truncation of the MOF particles: hexagonal bipyramidal MIL-96 particles (t = 0.24) rearranged into a 2D square lattice, whereas hexagonal bipyramidal MIL-96 particles (t = 0.52) self-assembled into centred rectangular lattices.[76]

6. Self-assembly of metal–organic framework particles into three-dimensional ordered superstructures

Self-assembly of MOF particles into 3D ordered superstructures was first achieved by sedimentation.[81] PVP-modified O-UiO-66 particles dispersed in water slowly settled by gravity in a glass capillary. After drying, UiO-66 particles were arranged into a hexagonal matrix to form compact oriented layers, which in turn were stacked on top of each other to generate 3D-ordered superstructures.[81] In 2018, our group demonstrated that cetyltrimethylammonium bromide (CTAB)-coated MOF colloidal particles can also self-assemble by water evaporation into different 3D lattices (Fig. 6(a)–(d)).[37] Using this strategy, TRD-ZIF-8 particles with a truncation (t) value greater than 0.66 were assembled into the densest rhombohedral packing, whereas those TRD-ZIF-8 particles with a lower t (<0.66) were organised into a fcc crystal. UiO-66 particles adopted a hexagonal lattice closely related to the Minkowski lattice. Remarkably, the use of this approach enabled the 3D assembly of MOF particles of different sizes, opening the door to create 3D photonic MOF super-crystals when particles sized *ca.* 200 nm (range: 178 ± 8 nm to 227 ± 10 nm) were used. Since ZIF-8 and UiO-66 particles that had been synthesised without CTAB did not exhibit ordered packing, it was suggested that this ionic surfactant balanced the van der Waals attractions between the MOF particles. Therefore, ionic surfactants have been postulated to be critical to stabilising the suspension and to preventing irreversible colloidal aggregation.[35,36] Thus, using this drying method, different (111)-, (100)-, and (110)-oriented fcc superstructures were recently assembled from TRD-ZIF-8 particles (t = 0.63) by adjusting the amount of surfactant CTAB in the colloidal solution.[95] The formation of less-dense packings was favoured by increasing the amount of surfactant. This was attributed to the ability of the surfactant to increase repulsive interactions during self-assembly and to decrease surface tension. Interestingly, the photonic properties of superstructures also were shown to depend on their growth orientation.[95,96]

The importance of surfactants in MOF self-assembly has been further demonstrated by Wang *et al*,[76] who found that surfactants could induce the attractive depletion force between MOF particles. Specifically, they observed the attractive depletion force as effective osmotic pressure, as two MOF particles in a solution containing surfactants moved closer to each other. This osmotic pressure ultimately caused the MOF particles to assemble. Recently, electric field followed by photopolymerization of trimethylolpropane triacrylate (TMPTA) also allowed the assembly and orientation of NU-1000, MIL-68(In) and MIL-53-NH_2(Al) rod-like particles into 3D MOF superstructures (Fig. 6(f)).[70] In this study, Chin *et al.* studied the importance of the aspect ratio of these rod-like MOF particles for their self-assembly, achieving well-ordered 3D MOF superstructures using rods with a length-to-diameter ratio ranging from 10 to 1.2.

7. Outlook

Colloidal particles spontaneously arrange into ordered superstructures *via* self-assembly. These particles can be viewed as building units for superstructures, just as atoms are for molecules. Today, MOFs can be considered to be a new type of

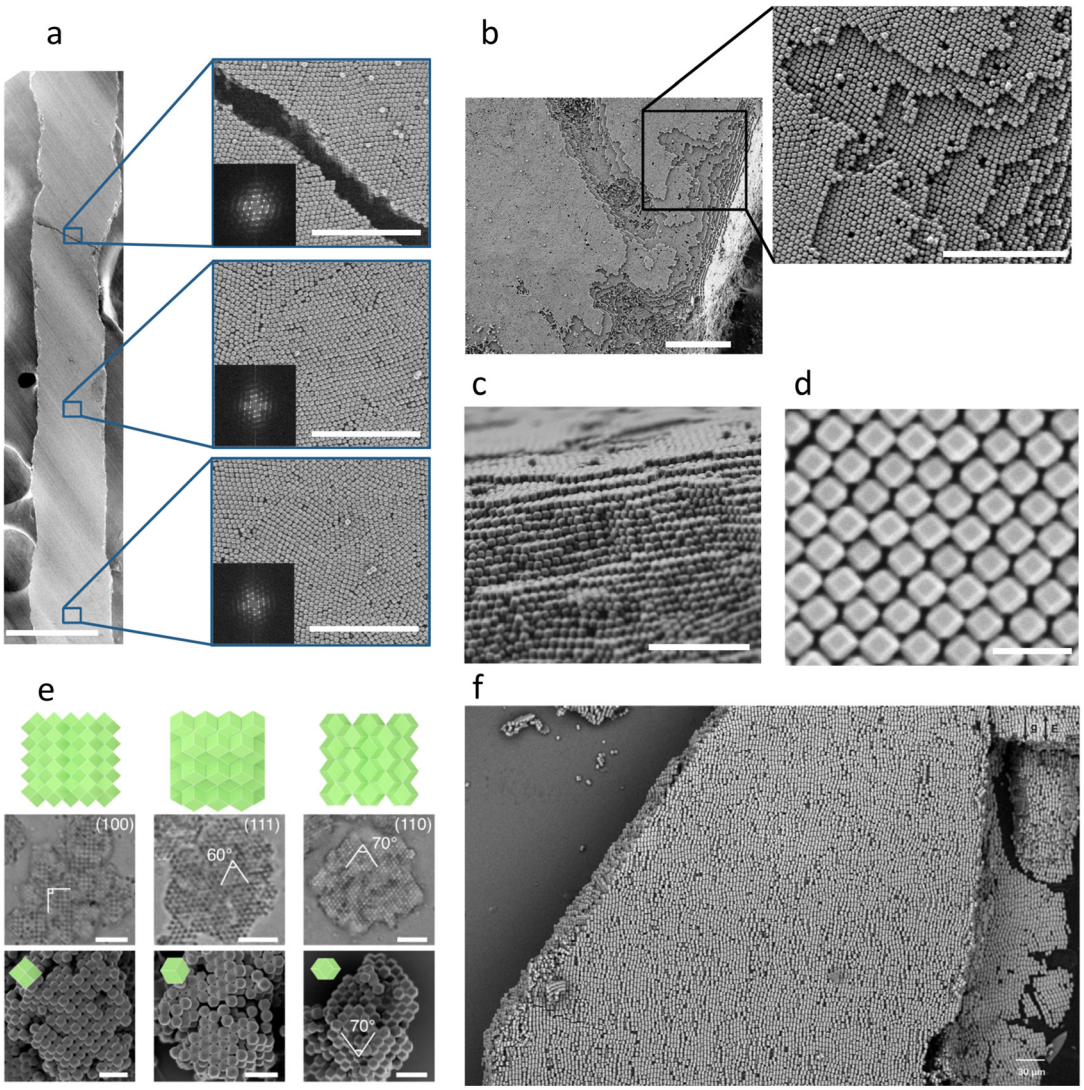

Fig. 6 (a)–(d) FE-SEM images of a 3D ordered rhombohedral superstructure made of TRD-ZIF-8 crystals (t = 0.69). Scale bars: (a) 200 μm; (a, insets) 5 μm; (b) 10 μm; (b, inset) 1 μm; (c) 2 μm; (d) 500 nm. Adapted with permission from ref. 37. Copyright 2017 Springer Nature. (e) Quasi-3D superstructures of RD-ZIF-8 particles formed on a rough substrate. (100)-, (111)-, and (110)-oriented colloidal crystals. Scale bars: (e) 5 μm for microscope images, and 2 μm for SEM images. Adapted with permission from ref. 76. Copyright 2022 Springer Nature. (f) SEM image of a 3D superstructure of MIL-68(In) particles made in a vertical E-field. Adapted with permission from ref. 70. Copyright 2022 Elsevier.

colloidal polyhedral particles for the assembly of superstructures (Table 1). This is mainly due to the recent synthetic advances in making them monodisperse in size and shape and in conferring them with high colloidal stability. Accordingly, we expect that further developments in the synthesis of monodispersed colloidal MOF particles, encompassing new MOFs and polyhedral shapes, will expand the gamut of accessible superstructures, thus opening the door to new packings and perhaps to more complex and even counterintuitive assemblies.

However, accessing new superstructures will require not only greater efforts in the synthesis of MOF particles, but also the improvement of their functionalisation (*e.g.* with oligonucleotides) and the development (or adaptation) of new strategies to induce their self-assembly. For example, inefficient entropic crystallisation caused by evaporation can lead to flocculation of MOFs. To circumvent this limitation, researchers could exploit depletion forces and/or external fields for evaporation-based assembly. Well-established self-assembly techniques for other colloidal particles could also be extrapolated to colloidal MOFs. For example, the assembly of MOF particles grafted with hydrocarbon-based polymers could be induced by slowly increasing the polarity of the colloidal solution.[58] Thinking one step further, one could imagine sophisticated monodisperse MOF particles with intrinsic assembly information that spontaneously drive the formation of superstructures, or the co-assembly of different polyhedral MOF particle to form multicomponent superstructures.

Yaghi, Wuttke, and co-workers have proposed a new strategy to self-assemble colloidal MOF particles into ordered

superstructures.[97,98] They theorised that the concepts and knowledge of reticular chemistry could be extended to structures within the macroscopic regime, referring to this concept as "augmented reticular chemistry". Therefore, they envisage that MOFs and COFs could serve as building units that would link together to form superstructures, analogously to how discrete molecular building blocks form MOFs and COFs. In doing so, superstructures with complex functionality could thus be designed with the precision of molecular chemistry. However, augmented reticular chemistry has yet to be reported experimentally.[97,98] Continued advances in synthetic techniques to control the interactions of MOF particles, as well as the interactions between MOF particles and their environment, will surely yield more complex superstructures.

Regarding the characterisation of MOF-based superstructures, the recent use of *in situ* imaging techniques, including confocal microscopy and *in situ* atomic force microscopy (AFM), enables real-time visualisation of self-assembly processes and consequently, exploration of the kinetics of self-assembly. Similarly, *in situ* small-angle X-ray scattering (SAXS) provides real-time information about the spatial arrangement of MOF particles. Therefore, conventional techniques such as scanning electron microscopy (SEM), transmission electron microscopy (TEM), scanning transmission electron microscopy (STEM), AFM, and SAXS all complement *in situ* techniques well.

Although the applications of superstructures made from colloidal MOF particles remain in their infancy, they hold great potential. MOF-based superstructures have been used primarily for photonics-related applications such as chemical sensing, thermal imaging, and anti-counterfeiting measures (Fig. 7). MOF particles can self-assemble into photonic crystals that reflect light at specific wavelengths and directions. The photonic bandgap of MOF-based superstructures depends on the size and orientation of the assembled MOF particles, the lattice spacing, the degree of internal order of the structures, and the adsorption of guest molecules.[59] Photonic MOF-based superstructures have been reported to detect the presence of C1–C8 alcohols (methanol, ethanol, isopropanol, *n*-butanol, *etc.*), and of C5–C8 linear alkanes and alkenes.[89] The adsorption of those species shifts the spectral position of the photonic bandgap of the structures, thus modifying their structural colours. Photonic superstructures have also been applied to local thermal and photothermal sensing. Specifically, MOF-based photonic supraparticles have been found to act as temperature probes in the presence of alcohol vapour.[60] The application range of photonic MOF-based superstructures has recently been extended to anticounterfeiting. The information can be encrypted by playing with the reflection signals of different superstructures.[99] Interestingly, birefringent 2D superstructures have been reported. These include 2D superstructures made of dye-adsorbed MOF particles of coordinated orientation, which exhibit anisotropic fluorescence, which may eventually expand the development of advanced materials for sensing, optics, or photonics.[76] MOF-based superstructures have also

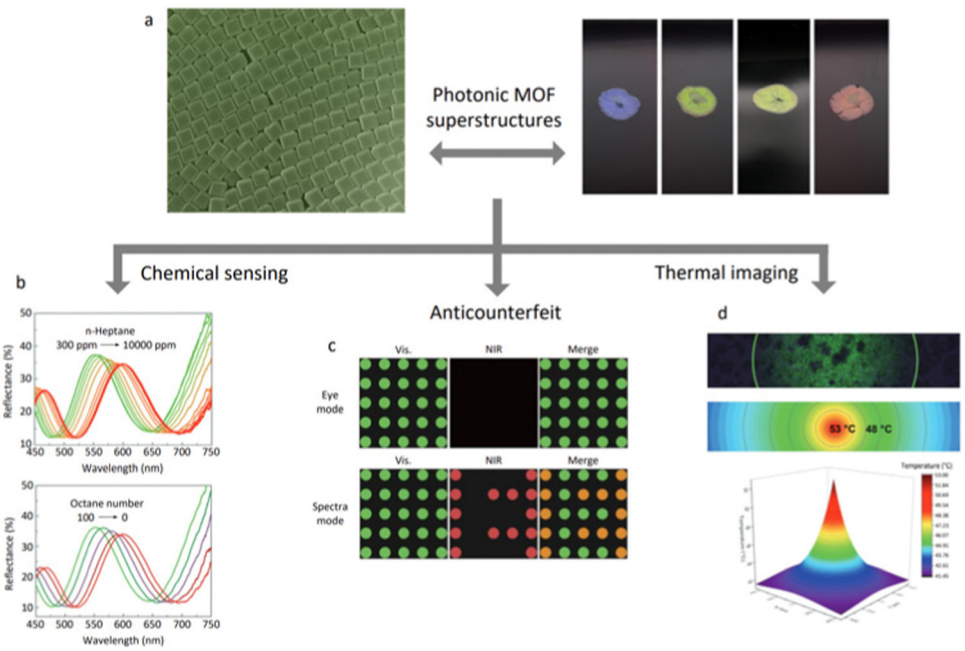

Fig. 7 Schematic illustration of photonics-related applications of MOF-based superstructures. (a) Photographs of 3D ordered superstructures made of TRD ZIF-8 particles of different sizes (178 ± 8 nm (blue); 193 ± 8 nm (green); 210 ± 10 nm (yellow); and 227 ± 10 nm (red)). Adapted with permission from ref. 37. Copyright 2017 Springer Nature. (b) Reflectance spectra of monolayers made of RD ZIF-8 as a function of exposure to 1-heptane vapour (up) and after exposure to simulated gasoline vapours with varying octane numbers (bottom). Adapted with permission from ref. 89. Copyright 2021 The Royal Society of Chemistry. (c) Information encryption by combining MOF-based superstructures with different lattices and thus photonic properties. Adapted with permission from ref. 99. Copyright 2021 John Wiley and Sons. (d) Hyperspectral and optical microscopy image of laser-irradiated ZIF-8 photonic balls (up) and its corresponding 2D (middle) and 3D (bottom) thermal map. Adapted with permission from ref. 60. Copyright 2021 John Wiley and Sons.

been harnessed for photocatalysis.[90] Specifically, 2D hexagonal lattices made of PCN-222 nanorods have shown photocatalytic activity towards the selective partial oxidation of 2-chloroethyl ethyl sulphide to the non-toxic compound 2-chloroethyl ethyl sulfoxide. These superstructures exhibited higher catalytic conversion efficiency compared to bulk PCN-222 crystals, which could be attributed to the higher photosensitisation efficiency associated with the superstructures.[90] Moreover, self-assembled MOF particles may benefit the countless applications for which MOFs offer promise, such as adsorption, separation, catalysis, and drug delivery.[100–109]

The practical exploitation of MOF-based superstructures is limited by their chemical stability and susceptibility to mechanical stress. The stability of MOF-based superstructures has not yet been extensively studied; therefore, the current data set is insufficient. However, the low mechanical stabilities of these superstructures is undeniable. Importantly, the molecular chains, which tether MOF particles and stabilise sterics, establish relatively weak interactions among neighbouring MOF particles. Logically, these weak interactions have a detrimental effect on the mechanical performance of MOF-based superstructures. Accordingly, a self-assembly strategy based on augmented reticular chemistry would ensure the stability of the superstructures, since this theoretical approach is based on the strong covalent bonding of the frameworks.[97,98] As Cohen *et al.* revealed, the stability of superstructures can also be improved by grafting the particles with a polymer of high molecular weight and density brush.[84] A similar approach was also used by Chin *et al.*, who photopolymerized TMPTA to fix the oriented MOF particles embedded within the photopolymer. However, to date, this approach could suffer from a trade-off between increasing mechanical stability and decreasing superstructure-order or inherent porosity of the embedded MOF particles. Thus, further studies on the mechanical behaviour of MOF-based superstructures—including measurements of hardness, elastic modulus, shear modulus, and yield strength—are needed to comprehensively understand the variables that influence their stability.

The field of MOF self-assembly presents many opportunities and challenges. For example, controlling the self-assembly of MOF particles remains a very challenging task. We believe that computational modelling may help with controlling the self-assembly process of MOF particles, guiding experimental synthesis efforts, and ultimately, designing new superstructures.[110] However, we recognise that this has not yet been reported in the literature. Therefore, we expect that theoretical predictions will accelerate advances in MOF particle self-assembly. Future work should aim to expand the set of MOF-based superstructures. Indeed, MOF particle self-assembly is restrained to highly symmetric structures such as microspheres, linear chains, periodic lattices, and periodic 3D structures.[37,59,71,79] The ability to design superstructures with dynamic behaviour that could rival those found in natural materials (*e.g.* muscle, wood, or cytoskeletons) perhaps remains a far-off goal. Research could also focus on expanding MOF-based superstructures through post-synthetic transformations, including calcination processes, to obtain superstructures with otherwise inaccessible properties.[94] Furthermore, post-synthetic transformations of these assemblies have not yet been reported, although similar chemistry has been done on homologous superstructures prepared by self-assembly of non-MOF building blocks.[58] Regardless, we are confident that the field of MOF self-assembly will continue to garner attention from the research community and is poised for growth and exciting advances.

Abbreviations

PMMA	Poly-(methyl methacrylate)
fcc	Face-centred cubic
hcp	Hexagonal close-packed
rhcp	Random hexagonal close-packed
3D	Three-dimensional
bcc	Body-centred cubic
MOF	Metal–organic framework
0D	Zero-dimensional
C-Fe-soc-MOF	Cubic Fe-soc-MOF
C-ZIF-8	Cubic ZIF-8
RD-ZIF-8	Rhombic dodecahedral ZIF-8
TRD-ZIF-8	Truncated rhombic dodecahedral ZIF-8
O-UiO-66	Octahedral UiO-66
PVP	Polyvinylpyrrolidone
1D	One-dimensional
o-TPM	3-(Trimethoxysilyl)propyl methacrylate
CTAC	Cetyltrimethylammonium chloride
2D	Two-dimensional
DMF	*N*,*N*-Dimethylformamide
LB	Langmuir–Blodgett
SDS	Sodium dodecyl sulphate
PMA	Poly-(methyl acrylate)
PBnMA	Poly-(benzyl methacrylate)
TC-ZIF-8	Truncated cubic ZIF-8
CTAB	Cetyltrimethylammonium bromide
t	Truncation
SEM	Scanning electron microscopy
TEM	Scanning electron microscopy
STEM	Scanning transmission electron microscopy
AFM	Atomic force microscopy
SAXS	Small-angle X-ray scattering
TMPTA	Trimethylolpropane triacrylate

Conflicts of interest

There are no conflicts to declare.

Acknowledgements

This work was supported by grant ref. PID2021-123265NB-I00 funded by MCIN/AEI/10.13039/501100011033/and by ''ERDF A way of making Europe''. It was also funded by the Catalan

AGAUR (project 2021 SGR 00458), and by the CERCA Program/Generalitat de Catalunya. ICN2 is supported by the Severo Ochoa program from the Spanish MINECO (grant no. SEV-2017-0706). L. Meng thanks the China Scholarship Council (CSC) for scholarship support (202106080019).

References

1 Y. Min, M. Akbulut, K. Kristiansen, Y. Golan and J. Israelachvili, *Nat. Mater.*, 2008, **7**, 527–538.
2 A. V. Pinheiro, D. Han, W. M. Shih and H. Yan, *Nat. Nanotechnol.*, 2011, **6**, 763–772.
3 K. A. Dill and J. L. MacCallum, *Science*, 2012, **338**, 1042–1046.
4 I. A. Chen and P. Walde, *Cold Spring Harbor Perspect. Biol.*, 2010, **2**, a002170.
5 G. Ragazzon and L. J. Prins, *Nat. Nanotechnol.*, 2018, **13**, 882–889.
6 G. A. Ozin, K. Hou, B. V. Lotsch, L. Cademartiri, D. P. Puzzo, F. Scotognella, A. Ghadimi and J. Thomson, *Mater. Today*, 2009, **12**, 12–23.
7 K. Thorkelsson, P. Bai and T. Xu, *Nano Today*, 2015, **10**, 48–66.
8 Z. Li, Q. Fan and Y. Yin, *Chem. Rev.*, 2022, **122**, 4976–5067.
9 Y. Lu, H. Fan, A. Stump, T. L. Ward, T. Rieker and C. J. Brinker, *Nature*, 1999, **398**, 223–226.
10 S. Wong, V. Kitaev and G. A. Ozin, *J. Am. Chem. Soc.*, 2003, **125**, 15589–15598.
11 C. B. Murray, C. R. Kagan and M. G. Bawendi, *Science*, 1995, **270**, 1335–1338.
12 P. V. Braun and P. Wiltzius, *Nature*, 1999, **402**, 603–604.
13 M. Mozafari, F. Moztarzadeh, A. M. Seifalian and L. Tayebi, *J. Lumin.*, 2013, **133**, 188–193.
14 D. Liu, C. Li, F. Zhou, T. Zhang, H. Zhang, X. Li, G. Duan, W. Cai and Y. Li, *Sci. Rep.*, 2015, **5**, 7686.
15 Y. Xia, B. Gates, Y. Yin and Y. Lu, *Adv. Mater.*, 2000, **12**, 693–713.
16 G. von Freymann, S. John, V. Kitaev and G. A. Ozin, *Adv. Mater.*, 2005, **17**, 1273–1276.
17 V. J. Anderson and H. N. W. Lekkerkerker, *Nature*, 2002, **416**, 811–815.
18 M. E. Leunissen, C. G. Christova, A.-P. Hynninen, C. P. Royall, A. I. Campbell, A. Imhof, M. Dijkstra, R. van Roij and A. van Blaaderen, *Nature*, 2005, **437**, 235–240.
19 Z. Cheng and M. R. Jones, *Nat. Commun.*, 2022, **13**, 4207.
20 B. Pietrobon, M. McEachran and V. Kitaev, *ACS Nano*, 2009, **3**, 21–26.
21 K. Miszta, J. de Graaf, G. Bertoni, D. Dorfs, R. Brescia, S. Marras, L. Ceseracciu, R. Cingolani, R. van Roij, M. Dijkstra and L. Manna, *Nat. Mater.*, 2011, **10**, 872–876.
22 J. J. Geuchies, C. van Overbeek, W. H. Evers, B. Goris, A. de Backer, A. P. Gantapara, F. T. Rabouw, J. Hilhorst, J. L. Peters, O. Konovalov, A. V. Petukhov, M. Dijkstra, L. D. A. Siebbeles, S. van Aert, S. Bals and D. Vanmaekelbergh, *Nat. Mater.*, 2016, **15**, 1248–1254.
23 S. Xie, X. Zhou, X. Han, Q. Kuang, M. Jin, Y. Jiang, Z. Xie and L. Zheng, *J. Phys. Chem. C*, 2009, **113**, 19107–19111.
24 J. J. Giner-Casares and J. Reguera, *Nanoscale*, 2016, **8**, 16589–16595.
25 M. Grzelczak, J. Vermant, E. M. Furst and L. M. Liz-Marzán, *ACS Nano*, 2010, **4**, 3591–3605.
26 F. Li, Z. Wang and A. Stein, *Angew. Chem., Int. Ed.*, 2007, **119**, 1917–1920.
27 F. Li, Y. Qian and A. Stein, *Chem. Mater.*, 2010, **22**, 3226–3235.
28 U. Agarwal and F. A. Escobedo, *Nat. Mater.*, 2011, **10**, 230–235.
29 A. P. Gantapara, J. de Graaf, R. van Roij and M. Dijkstra, *Phys. Rev. Lett.*, 2013, **111**, 015501.
30 A. Haji-Akbari, M. Engel, A. S. Keys, X. Zheng, R. G. Petschek, P. Palffy-Muhoray and S. C. Glotzer, *Nature*, 2009, **462**, 773–777.
31 S. Torquato and Y. Jiao, *Nature*, 2009, **460**, 876–879.
32 M. Rycenga, J. M. McLellan and Y. Xia, *Adv. Mater.*, 2008, **20**, 2416–2420.
33 J. Kim, M. R. Jones, Z. Ou and Q. Chen, *ACS Nano*, 2016, **10**, 9801–9808.
34 C.-W. Liao, Y.-S. Lin, K. Chanda, Y.-F. Song and M. H. Huang, *J. Am. Chem. Soc.*, 2013, **135**, 2684–2693.
35 K. L. Young, M. L. Personick, M. Engel, P. F. Damasceno, S. N. Barnaby, R. Bleher, T. Li, S. C. Glotzer, B. Lee and C. A. Mirkin, *Angew. Chem., Int. Ed.*, 2013, **52**, 13980–13984.
36 J. Henzie, M. Grünwald, A. Widmer-Cooper, P. L. Geissler and P. Yang, *Nat. Mater.*, 2012, **11**, 131–137.
37 C. Avci, I. Imaz, A. Carné-Sánchez, J. A. Pariente, N. Tasios, J. Pérez-Carvajal, M. I. Alonso, A. Blanco, M. Dijkstra, C. López and D. Maspoch, *Nat. Chem.*, 2018, **10**, 78–84.
38 N. Yanai and S. Granick, *Angew. Chem., Int. Ed.*, 2012, **51**, 5638–5641.
39 J. Troyano, A. Carné-Sánchez, C. Avci, I. Imaz and D. Maspoch, *Chem. Soc. Rev.*, 2019, **48**, 5534–5546.
40 O. D. Velev and S. Gupta, *Adv. Mater.*, 2009, **21**, 1897–1905.
41 M. Sindoro, N. Yanai, A.-Y. Jee and S. Granick, *Acc. Chem. Res.*, 2014, **47**, 459–469.
42 Q. Li, U. Jonas, X. S. Zhao and M. Kappl, *Asia-Pac. J. Chem. Eng.*, 2008, **3**, 255–268.
43 K. J. M. Bishop, C. E. Wilmer, S. Soh and B. A. Grzybowski, *Small*, 2009, **5**, 1600–1630.
44 C.-A. Palma, M. Cecchini and P. Samorì, *Chem. Soc. Rev.*, 2012, **41**, 3713–3730.
45 J. Zhang, Y. Li, X. Zhang and B. Yang, *Adv. Mater.*, 2010, **22**, 4249–4269.
46 C. Yi, S. Zhang, K. T. Webb and Z. Nie, *Acc. Chem. Res.*, 2017, **50**, 12–21.
47 N.-N. Zhang, X. Shen, K. Liu, Z. Nie and E. Kumacheva, *Acc. Chem. Res.*, 2022, **55**, 1503–1513.
48 R. Kubota, W. Tanaka and I. Hamachi, *Chem. Rev.*, 2021, **121**, 14281–14347.
49 C. Li, X. Qin, Z. Zhang, Y. Lv, S. Zhang, Y. Fan, S. Liang, B. Guo, Z. Li, Y. Liu and D. Luo, *Nano Today*, 2022, **42**, 101354.

50 Z. Cai, Z. Li, S. Ravaine, M. He, Y. Song, Y. Yin, H. Zheng, J. Teng and A. Zhang, *Chem. Soc. Rev.*, 2021, **50**, 5898–5951.
51 F. Yang, H. Mu, C. Wang, L. Xiang, K. X. Yao, L. Liu, Y. Yang, Y. Han, Y. Li and Y. Pan, *Chem. Mater.*, 2018, **30**, 3467–3473.
52 J. Cravillon, R. Nayuk, S. Springer, A. Feldhoff, K. Huber and M. Wiebcke, *Chem. Mater.*, 2011, **23**, 2130–2141.
53 W. Morris, S. Wang, D. Cho, E. Auyeung, P. Li, O. K. Farha and C. A. Mirkin, *ACS Appl. Mater. Interfaces*, 2017, **9**, 33413–33418.
54 C. Avci, J. Ariñez-Soriano, A. Carné-Sánchez, V. Guillerm, C. Carbonell, I. Imaz and D. Maspoch, *Angew. Chem., Int. Ed.*, 2015, **127**, 14625–14629.
55 E. P. K. Currie, W. Norde and M. A. Cohen Stuart, *Adv. Colloid Interface Sci.*, 2003, **100**, 205–265.
56 K. M. L. Taylor, W. J. Rieter and W. Lin, *J. Am. Chem. Soc.*, 2008, **130**, 14358–14359.
57 S. Ding, Y. Zhang, F. Lou, M. K. Aslam, Y. Sun, M. Li, J. Duan, Y. Li and S. Chen, *J. Mater. Chem. A*, 2022, **10**, 20813–20818.
58 M. A. Boles, M. Engel and D. V. Talapin, *Chem. Rev.*, 2016, **116**, 11220–11289.
59 J. Wang, Y. Liu, G. Bleyer, E. S. A. Goerlitzer, S. Englisch, T. Przybilla, C. Fru Mbah, M. Engel, E. Spiecker, I. Imaz, D. Maspoch and N. Vogel, *Angew. Chem., Int. Ed.*, 2022, **61**, e202117455.
60 C. Avci, M. L. De Marco, C. Byun, J. Perrin, M. Scheel, C. Boissière and M. Faustini, *Adv. Mater.*, 2021, **33**, 2104450.
61 M. Pang, A. J. Cairns, Y. Liu, Y. Belmabkhout, H. C. Zeng and M. Eddaoudi, *J. Am. Chem. Soc.*, 2013, **135**, 10234–10237.
62 A. D. Dinsmore, M. F. Hsu, M. G. Nikolaides, M. Marquez, A. R. Bausch and D. A. Weitz, *Science*, 2002, **298**, 1006–1009.
63 O. D. Velev, A. M. Lenhoff and E. W. Kaler, *Science*, 2000, **287**, 2240–2243.
64 A. Carné-Sánchez, I. Imaz, M. Cano-Sarabia and D. Maspoch, *Nat. Chem.*, 2013, **5**, 203–211.
65 J. Troyano, C. Çamur, L. Garzón-Tovar, A. Carné-Sánchez, I. Imaz and D. Maspoch, *Acc. Chem. Res.*, 2020, **53**, 1206–1217.
66 Y. Liu, J. Wang, I. Imaz and D. Maspoch, *J. Am. Chem. Soc.*, 2021, **143**, 12943–12947.
67 Z. Gong, T. Hueckel, G.-R. Yi and S. Sacanna, *Nature*, 2017, **550**, 234–238.
68 F. Cheng, A. J. Young, J.-S. G. Bouillard, N. T. Kemp, R. Guillet-Nicolas, C. H. Hall, D. Roberts, A. H. Jaafar, A. M. Adawi, F. Kleitz, A. Imhof, M. R. Reithofer and J. M. Chin, *J. Am. Chem. Soc.*, 2019, **141**, 12989–12993.
69 F. Cheng, E. S. Marshall, A. J. Young, P. J. Robinson, J.-S. G. Bouillard, A. M. Adawi, N. A. Vermeulen, O. K. Farha, M. R. Reithofer and J. M. Chin, *Chem. – Eur. J.*, 2017, **23**, 15578–15582.
70 K. Allahyarli, M. R. Reithofer, F. Cheng, A. J. Young, E. Kiss, T. T. Y. Tan, A. Prado-Roller and J. M. Chin, *J. Colloid Interface Sci.*, 2022, **610**, 1027–1034.
71 N. Yanai, M. Sindoro, J. Yan and S. Granick, *J. Am. Chem. Soc.*, 2013, **135**, 34–37.
72 S. Basuray and H.-C. Chang, *Phys. Rev. E: Stat., Nonlinear, Soft Matter Phys.*, 2007, **75**, 060501.
73 M.-T. Wei, J. Junio and H. D. Ou-Yang, *Biomicrofluidics*, 2009, **3**, 012003.
74 Y. Wang, Y. Wang, D. R. Breed, V. N. Manoharan, L. Feng, A. D. Hollingsworth, M. Weck and D. J. Pine, *Nature*, 2012, **491**, 51–55.
75 D. Lyu, W. Xu and Y. Wang, *Angew. Chem., Int. Ed.*, 2022, **61**, e202115076.
76 D. Lyu, W. Xu, J. E. L. Payong, T. Zhang and Y. Wang, *Nat. Commun.*, 2022, **13**, 3980.
77 K. L. Young, M. R. Jones, J. Zhang, R. J. Macfarlane, R. Esquivel-Sirvent, R. J. Nap, J. Wu, G. C. Schatz, B. Lee and C. A. Mirkin, *Proc. Natl. Acad. Sci. U. S. A.*, 2012, **109**, 2240–2245.
78 J. Kim, X. Song, F. Ji, B. Luo, N. F. Ice, Q. Liu, Q. Zhang and Q. Chen, *Nano Lett.*, 2017, **17**, 3270–3275.
79 M. Pang, A. J. Cairns, Y. Liu, Y. Belmabkhout, H. C. Zeng and M. Eddaoudi, *J. Am. Chem. Soc.*, 2012, **134**, 13176–13179.
80 Y. Katayama, M. Kalaj, K. S. Barcus and S. M. Cohen, *J. Am. Chem. Soc.*, 2019, **141**, 20000–20003.
81 G. Lu, C. Cui, W. Zhang, Y. Liu and F. Huo, *Chem. – Asian J.*, 2013, **8**, 69–72.
82 M. Tsotsalas, A. Umemura, F. Kim, Y. Sakata, J. Reboul, S. Kitagawa and S. Furukawa, *J. Mater. Chem.*, 2012, **22**, 10159–10165.
83 S. Motoyama, R. Makiura, O. Sakata and H. Kitagawa, *J. Am. Chem. Soc.*, 2011, **133**, 5640–5643.
84 K. Barcus, P.-A. Lin, Y. Zhou, G. Arya and S. M. Cohen, *ACS Nano*, 2022, **16**, 18168–18177.
85 P. A. Kralchevsky and K. Nagayama, *Langmuir*, 1994, **10**, 23–36.
86 E. P. Lewandowski, M. Cavellaro, L. Botto, J. C. Bernate, V. Garbin and K. J. Stebe, *Langmuir*, 2010, **26**, 15142–15154.
87 P. Yang and F. Kim, *ChemPhysChem*, 2002, **3**, 503–506.
88 K. D. Danov and P. A. Kralchevsky, *Adv. Colloid Interface Sci.*, 2010, **154**, 91–103.
89 S. Yu, X. Wang, X. Jiao, C. Li and D. Chen, *J. Mater. Chem. C*, 2021, **9**, 5379–5386.
90 S. Wang, S. S. Park, C. T. Buru, H. Lin, P.-C. Chen, E. W. Roth, O. K. Farha and C. A. Mirkin, *Nat. Commun.*, 2020, 11.
91 R. J. Macfarlane, B. Lee, M. R. Jones, N. Harris, G. C. Schatz and C. A. Mirkin, *Science*, 2011, **334**, 204–208.
92 M. R. Jones, N. C. Seeman and C. A. Mirkin, *Science*, 2015, **347**, 1260901.
93 W. B. Rogers, W. M. Shih and V. N. Manoharan, *Nat. Rev. Mater.*, 2016, **1**, 16008.
94 Y. Song, X. Song, X. Wang, J. Bai, F. Cheng, C. Lin, X. Wang, H. Zhang, J. Sun, T. Zhao, H. Nara, Y. Sugahara, X. Li and Y. Yamauchi, *J. Am. Chem. Soc.*, 2022, **144**, 17457–17467.
95 C. Avci, Y. Liu, J. A. Pariente, A. Blanco, C. Lopez, I. Imaz and D. Maspoch, *Small*, 2019, **15**, 1902520.
96 P. D. García, J. F. Galisteo-López and C. López, *Appl. Phys. Lett.*, 2005, **87**, 201109.
97 Z. Ji, R. Freund, C. S. Diercks, P. Hirschle, O. M. Yaghi and S. Wuttke, *Adv. Mater.*, 2021, **33**, 2103808.

98 J. Andreo, R. Ettlinger, O. Zaremba, Q. Peña, U. Lächelt, R. Fernández de Luis, R. Freund, S. Canossa, E. Ploetz, W. Zhu, C. S. Diercks, H. Gröger and S. Wuttke, *J. Am. Chem. Soc.*, 2022, **144**, 7531–7550.
99 S. Chen, D. Bu, Y. Hu, X. Xiao, D. Yang, D. Ma and S. Huang, *Adv. Photonics Res.*, 2021, **3**, 2100246.
100 L.-Z. Cai, Z.-Z. Yao, S.-J. Lin, M.-S. Wang and G.-C. Guo, *Angew. Chem., Int. Ed.*, 2021, **60**, 18223–18230.
101 J. Fonseca and S. Choi, *Inorg. Chem.*, 2020, **59**, 3983–3992.
102 H. Fan, M. Peng, I. Strauss, A. Mundstock, H. Meng and J. Caro, *Nat. Commun.*, 2021, **12**, 38.
103 Z. Niu, X. Cui, T. Pham, G. Verma, P. C. Lan, C. Shan, H. Xing, K. A. Forrest, S. Suepaul, B. Space, A. Nafady, A. M. Al-Enizi and S. Ma, *Angew. Chem., Int. Ed.*, 2021, **133**, 5343–5348.
104 Y. Shen, T. Pan, L. Wang, Z. Ren, W. Zhang and F. Huo, *Adv. Mater.*, 2021, **33**, 2007442.
105 J. Fonseca and S. Choi, *Catal. Sci. Technol.*, 2020, **10**, 8265–8282.
106 S. Mallakpour, E. Nikkhoo and C. M. Hussain, *Coord. Chem. Rev.*, 2022, **451**, 214262.
107 H. D. Lawson, S. P. Walton and C. Chan, *ACS Appl. Mater. Interfaces*, 2021, **13**, 7004–7020.
108 J. F. Olorunyomi, S. T. Geh, R. A. Caruso and C. M. Doherty, *Mater. Horiz.*, 2021, **8**, 2387–2419.
109 D. Luo, C. Li, Y. Zhang, Q. Ma, C. Ma, Y. Nie, M. Li, X. Weng, R. Huang, Y. Zhao, L. Shui, X. Wang and Z. Chen, *Adv. Mater.*, 2022, **34**, 2105541.
110 M. Dijkstra and E. Luijten, *Nat. Mater.*, 2021, **20**, 762–773.